Flutter mitigation of turbofan blades using viscoelastic patches

B. Manayil Santhosh [1], M. Tufekci[2], L. Salles [2], F. Scarpa[3], J. Yuan [1,2]
[1] University of Strathclyde, Department of Mechanical and Aerospace Engineering,
Aerospace Centre of Excellence,
Glasgow, G1 1XQ, UK
e-mail: **jie.yuan@strath.ac.uk**

[2] Imperial College London, Department of Mechanical Engineering, Dynamics Group,
London, SW7 2AZ, UK

[3] University of Bristol, Department of Aerospace Engineering, Bristol Composite Institute,
Bristol, BS1 1TH, UK

Abstract
Flutter as a self-feeding aeroelastic instability presents one of the biggest challenges in aero-engine designs to improve its aerodynamic and structural performance. This work presents a detailed feasibility study of using different viscoelastic patches as Constrained Layer Damping (CLD) enhancement for an aero-engine fan blade to reduce potential flutter risks. The static and dynamic responses of the different materials and configurations (thicknesses, layers and locations) are evaluated on both cruise and take-off/landing conditions. It is found that a double bi-layer 3M® ISD110 is the optimal choice of material for the CLD treatment for the fan blade. The study also shows that an optimal CLD treatment of 15 % total surface area of the blade at the root demonstrated a 36 % reduction in resonance amplitudes across the first six modes.

1 Introduction

The demand for lighter, cleaner and more efficient propulsion systems in the aerospace industry has driven the design and manufacture of constituent components to their structural limits. The most pervasive type of aircraft powerplant is the turbofan jet engine. When the turbofan was introduced, it had lower bypass ratios in the range of 0.5- 2. It has grown consistently up to 10 over the years, creating classes of its own, namely, high bypass turbofan and ultra-high bypass turbofan [1]. The bypass ratio is defined as the ratio of air that gets bypassed through the bypass nozzle to that through the core. The bypass duct contributes to more than 80% of the overall thrust produced by the engine, while the core produces the heat energy to supply power to run the compressor and the turbofan spool via turbines contributes much less to the thrust. As the core uses combustion energy through aviation fuel (fossil fuel) combustion, the major operational objective is to yield maximum thrust for minimum fuel consumption [2]. The turbine blades are subjected to a variety of static and dynamic stresses during their operation. The static stresses are a result of thermal gradients, centrifugal loads and fluid pressure perturbations or a combination of all the above. The dynamics stresses are a result of mechanical and aerodynamic vibrations such as resonant or non-resonant vibrations on engine structure and aero-mechanical instabilities and perturbations in the pressure-flow field, which negatively affect the High Cycle Fatigue (HCF) life of the component. Vibration-induced HCF failure is widely regarded as the main reason for aircraft powerplant failure, particularly in the case of jet engines [3]. Jet engines rotate at a higher RPM than the propeller engines, and as a result, high cycle loading is a major cause of fatigue failures in this class of engines; as explained in Rao [4] that high-cycle fatigue is also caused due to flow-induced vibrations. Resonance occurs when the external periodic loading on the mechanical

This is an accepted author manuscript of the following conference contribution: Manayil Santhosh, B., Tufekci, M., Salles, L., Scarpa, F., & Yuan, J. (2022). Flutter mitigation of turbofan blades using viscoelastic patches. Paper presented at Proceedings of ISMA 2022 - International Conference on Noise and Vibration Engineering and USD 2022 - International Conference on Uncertainty in Structural Dynamics.

system equals any one of the major natural frequencies of the structure. They cannot be completely removed in bladed disc systems because of a number of resonance crossings in the Campbell diagram [5], which is used to predict the preliminary crossings of the resonant vibrations with the external cyclic vibrations. Fan blade systems provide more than 80% of the thrust for the aerospace propulsion system assembled through several flexible blades that are very sensitive/vulnerable to HCF. The increase in bypass ratio for improved propulsion efficiency in the aero-engine makes the diameter of the fan blade system significantly larger than before, leading to high modal density in fan blades that are much more susceptible to vibrations under a wide range of operational conditions [6]–[13]. To guarantee the reliability and durability of aero-engine components, the vibrations arising in the powerplant system must be reduced effectively.

Generally speaking, the primary vibration damping techniques employed in an aero-engine are friction damping and material damping. Friction damping are employed to mitigate the vibrations that arise due to joint connections and ensure enhanced vibration energy dissipation. It is essentially a kind of nonlinear damping models as suggested in [14]. The common locations where it can be applied are the interface between the hub and the 'blisk' (industry term for the blade and the disk of the compressor fan blades in a turbofan) such a case using a NASA Rotor 67 is discussed in detail in [14],[15]. They are widely regarded as the most common damping method in the aircraft engines, in the fan blade system, the HP compressor blisk and likewise [14]–[16]. Piezo-electric damping can be also used in fan blade systems for active damping control by tuning the system electronically through external power to suppress the resonant vibrations [17]. However, active damping being external power-dependent is practically hard to implement due to the wiring and electronics involved. Passive vibration damping methods like contact friction methods although effective do not find much applications on turbofan blades because of large centrifugal loading that prevents effective slipping between contact interfaces in the joints.

Viscoelastic vibration damping is basically a passive damping treatment in which the shear deformational energy is dissipated, and the consequential heating effect causes vibration damping by strain energy dissipation. The viscoelastic damping method does not depend on any external power source to dissipate energy, and the damping is an inherent property of the material, making it a 'self-sufficient' damping treatment [18]. Moreover, it is demonstrated to be capable of coupling with active damping techniques such as piezoelectric damping techniques to improve the damping performance of the untuned damping treatment [19]–[21]. This interchangeability and relative cost-effectiveness make viscoelastic material damping the primary damping treatment for the purpose of this research. Viscoelastic materials have good damping properties because of their property to dissipate strain energy which makes them ideal for damping treatments. The damping property of the viscoelastic materials is both temperature and frequency-dependent. The strain energy of the baseline structure layer, which is in contact with the viscoelastic layer, causes a rise in the intermolecular frictional forces within the viscoelastic layer leading to strain energy dissipation [22]. The application of viscoelastic material on the turbofan blade can be made in broadly two configurations; the Free Layer Damping (FLD) method and the Constrained Layer Damping (CLD) method. As expected, FLD configuration can increase damping performance with an increase in the FLD thickness and patch area. However, for the purpose of this research, the FLD configuration is not considered mainly due to the following two reasons. Firstly, the weight and cost/benefit ratio obtained from cost-benefit analysis from FLD is much lower than the CLD for a given area. Secondly, the aerodynamic performance of the fan blade structure can be more affected by the increase of thickness in FLD. CLD employs an additional layer comprising a highly elastic material that is used to sandwich the viscoelastic layer between itself and the base structure. This extra layer, known as the constraining layer, induces shear deformation in the viscoelastic layer and increases strain energy dissipation from the base structure. The primary design parameters of CLD are the location of the viscoelastic damping patch, the thickness of the viscoelastic layer, the thickness of the constraining layer and the number of layers.

As discussed, there are many methods to reduce aero-engine vibrations that could be based on either active or passive damping, such as friction dampers and piezoelectric patches. In this paper, the objective of this paper is to investigate the feasibility of using viscoelastic vibration-damping patches to mitigate aeroelastic flutter and vibrations on fan blades. A study of using a viscoelastic passive damping layer for vibration mitigation in a fan blade system is presented. CLD combining the viscoelastic and constraining layer is used to provide effective shear deformation-induced damping. It is also found that very few studies are focused on optimum damping treatment using multiple layers of CLD for flutter mitigation of turbofan blades due

to the challenges of structural and aerodynamical modelling. This research will bridge the gap between the simple plate/beam models by taking a 3D full-scale finite element meshing strategy to incorporate the constrained viscoelastic damping treatments. In this study, a finite element model of fan blade is used to numerically investigate the effectiveness of these dampers as a case study. It will also explore the material properties of different viscoelastic patches and optimises the configuration of the patches on aero-engine turbo-fan blades. The study achieves the following five specific objectives: (1) review literature on the various viscoelastic patches available in the market, highlighting key mechanical properties; (2) elicit the modal participation factor summary to find the number of modes required to be considered for the forced frequency response analysis; (3) establish the baseline behaviour of the turbofan blade by performing static structural, modal and harmonic frequency analysis; (4) develop a patch material selection strategy with the aid of modal and harmonic response(dynamic) analysis of the turbo-fan blades with the patches; (5) perform the static and dynamic analyses for the cruise and take-off temperature conditions.

2 Finite element modelling

2.1 Geometry

Figure 1 and 2 represents the top view of the turbofan blade and the front view of the turbofan blade with the annotated dimensions. The turbofan geometry is modelled in the Solidworks CAD environment. The main dimensions of the fan blade available in open-source literature are used to create the model in Solidworks. The constraining layer thickness is considered to be 0.135 mm and the viscoelastic layer thickness to be 0.135 mm to maintain the same thickness ratio which is schematically displayed in Figure 3. The thickness ratio of 1 is found to be optimal when the cost associated with increased thickness of the constraining layer is not a major cause of concern [22], [24].

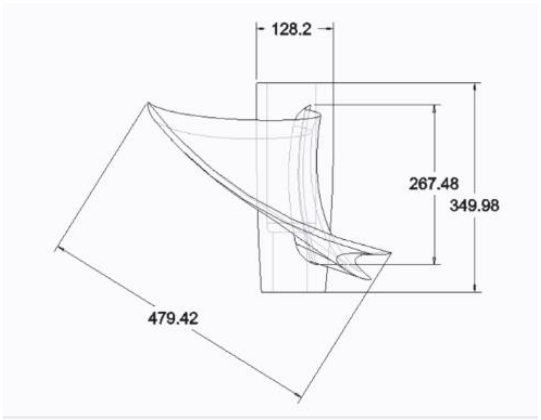

Figure 1: Top view of the fan blade

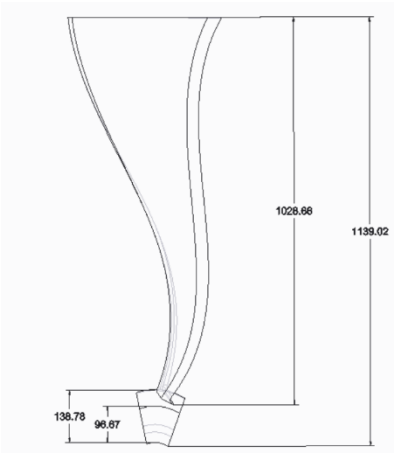

Figure 2: Front view of the fan blade

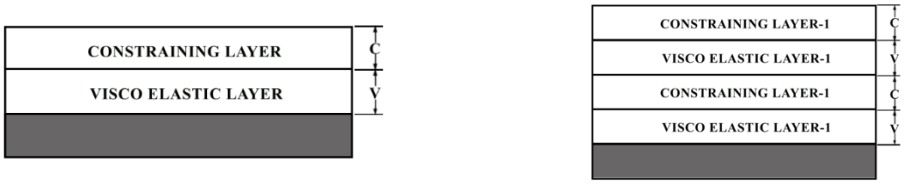

Figure 3: Cross-sections of single bi-layer and double bi-layer constrained layer damping

2.2 Discretisation and mesh convergence studies

In the finite element analysis problems, where highly elastic and plastic structural domains are present, the hexahedral mesh is proven to be more beneficial. Hexahedral mesh provides reduced error, smaller element counts, and improved reliability as compared to tetrahedral mesh [23]. Due to these benefits, a hexahedral type of mesh is chosen for meshing the solid rectangular bracket. While meshing, shell elements are not considered for the fan blade model as the model in the study is a complicated turbofan blade. The shell elements when applied on a heavily 3D dominated model, are known to cause computational errors while solver evaluation due to shear locking. For the modelling of the turbofan blade, hexahedral elements are considered with an outer tetrahedral layer of elements because it captures the shear deformation better than hexahedral elements alone. For the constrained layer and viscoelastic layer modelling, shell elements are used. Considering their low thicknesses, the normal and especially shear stress distribution throughout their cross-section can be accurately represented using the shell elements without introducing an extra computational cost to the model. The Quad4 with rigid link offset is used. The geometry of the blade is imported in IGES file format, and the meshing is performed using the ANSYS Mechanical solver. Hex-dominant meshing is adopted as per the discussion in section 5.3. and the obtained mesh is shown in Figure 4.

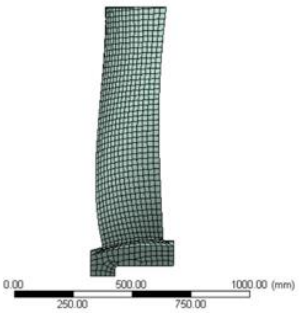

Figure 4: Baseline turbofan blade mesh depicting hexahedral elements

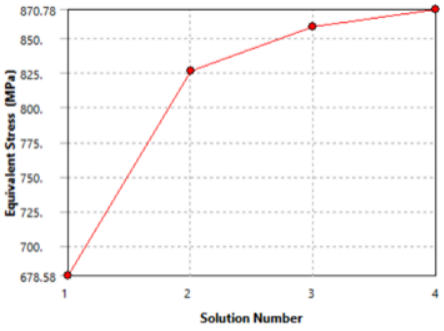

Figure 5: Mesh convergence study for four refinement levels

As the DOF of a system increases, the accuracy of the solution also increases [25]. However, a higher indicated DOF could result in a prolonged solver time required. Therefore, a trade-off between solver time and the accuracy of the solutions is opted for in order to arrive at an optimal solution. Mesh convergence assesses the number of mesh elements needed to ensure that the results have converged. The system response considered in this case is the equivalent (Von-Mises) stress developed on the blade. A preliminary mesh convergence study is done to assess whether the structure was ill-constrained. The convergence study is represented in Figure 5. Four refinement levels are selected by the solver for the convergence studies. It is observed that the solution converged at 870.78 MPa, where the per cent change with the preceding refinement level is 1.43%.

2.3 Pressure distribution

The pressure distribution is found using a polynomial function applied on both the fan blade's pressure side and the suction side. This is extracted from the CFD solver with a rotational velocity of 2500 RPM [26]. The pressure side polynomial function is a 6^{th}-degree polynomial in 2 variable coordinates, x and y. Since circular symmetry is applied for the analysis to consider the rotational velocity of the blade, the cartesian coordinate is transformed into a radial coordinate system with r representing the radial distance from the root and the z representing the length from the fore to the aft of the engine. The pressure distribution on both sides of the fan blade is visualised in Figure 6.

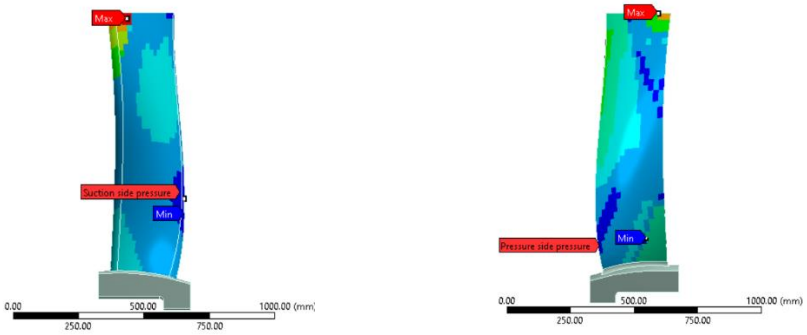

Figure 6: Suction side (left) and Pressure side pressure distribution over the fan blade

2.4 Operation temperature

The operating conditions of the fan blade structure need to be considered to model the system's dynamic response since viscoelastic materials' damping properties depend on the temperature. In this study, the fan blade dynamics are investigated in sea-level temperature during the take-off, and landing stages and cruise temperature that could drop to an interval between -30°C to -65°C as the typical commercial aircraft usually operates between 31,000 and 38,000 feet [9]. It is, therefore, imperative to consider altitude variations for modelling the vibrational response of the aircraft engine with viscoelastic polymers, which are temperature-dependent as well as frequency-dependent [10], [11], [12]. [13].

2.5 Material properties of the fan blade and viscoelastic patches

A homogenous blade structure is assumed for this study since the blade has a complex geometry. The material properties of the baseline turbofan structure, including the mechanical and damping properties of the Titanium alloy Ti-6Al-4V with Young's modules of 96 GPa. For viscoelastic materials considered in this study, namely 3M467, 3M ISD-110 and Sound coat N5, the loss factor (η) can be obtained through the loss (E'') and storage moduli (E') as shown in Equation 1. Table 1 shows these three viscoelastic materials' loss factors and complex modulus. In contrast, Table 2 shows an example of the mechanical properties of the constrained damping layer with 3M ISD-467 that can be directly defined in ANSYS.

$$\eta = 1 - \frac{(E' + E'')}{E'} \tag{1}$$

Table 1: Material properties of viscoelastic materials

Material Name		3M467 adhesive layer	3M ISD-110 adhesive layer	Sound coat N5 adhesive layer
Density / g/cm^3		0.9-1.0	0.9-1.0	1.049
Young's Modulus [MPa]	-40°C	-	-	-
	30°C	-	-	-
Shear modulus [MPa]	-40°C	100	50.11	199.52
	30°C	0.98	0.50	0.631
Loss Factor η	-40°C	0.20	0.55	0..20
	30°C	1.02	1.17	0.23

Table 2: An example of mechanical properties of the constrained damping layer

Material	Temperatue	G/MPa /E/GPa	Density kg/m^3	Poisson's ratio	Strength
3M ISD-467 damping layer	-40 degrees	100	0.9-1.0	0.49	-
	30 degrees	0.98	0.9-1.0	0.49	-
Aluminum 2024-T6	-40 degrees	64000	2695	0.32	415MPa
	30 degrees		-		

3 Modelling approach

3.1 Modal analysis

The general equation of motion of the system is represented in Equation 2. To identify the free vibration characteristics of the fan blade, a linear modal analysis procedure is followed to retrieve the modal properties of the system, namely natural frequency and the mode shapes of the fan blade system. To extract the eigenmodes of the system, an undamped modal analysis is performed. Therefore, the damping matrix $[\boldsymbol{C}]$ is initially not considered.

$$[\boldsymbol{M}]\{\ddot{\boldsymbol{u}}\} + [\boldsymbol{C}]\{\dot{\boldsymbol{u}}\} + [\boldsymbol{K}]\{\boldsymbol{u}\} = \boldsymbol{f}(\boldsymbol{t}) \quad (2)$$

$$([\boldsymbol{K}] - \boldsymbol{\omega_i}^2[\boldsymbol{M}])\{\emptyset\}_{\boldsymbol{i}} = \{\boldsymbol{0}\} \quad (3)$$

The angular frequency of the fan blade system is represented by $\boldsymbol{\omega_i}$ and $\{\emptyset\}_{\boldsymbol{i}}$ denotes the maximum amplitude or the mode shape corresponding to the natural frequency of the system, which is denoted in Equation 3. The mode shapes indicate the deformation regimes of the structure at different eigenmodes or natural frequencies.

3.2 Harmonic response analysis

As shown in Equation 4, harmonic response analysis is used to obtained the steady-state response of the fan blade system across a wide range of excitation frequencies because fan blade systems is commonly subjected to periodical engine order excitation.

$$(-\boldsymbol{\Omega^2}[\boldsymbol{M}] + \boldsymbol{i\Omega}[\boldsymbol{C}] + [\boldsymbol{K}]) \times (\{\boldsymbol{u_1}\} + \boldsymbol{i}\{\boldsymbol{u_2}\}) = (\{\boldsymbol{F_1}\} + \boldsymbol{i}\{\boldsymbol{F_2}\}) \quad (4)$$

The complex modal coordinate vector represented as the modal contribution vector is integrated over the number of modes to compute the displacement.

The harmonically exciting force is represented in Equation 5 and it is used to input the excitation force for time ***t:***

$$\boldsymbol{F_i} = \boldsymbol{F_i}\, \boldsymbol{sin}(\boldsymbol{\Omega_i t} + \boldsymbol{\theta_i}) \quad (5)$$

4 Results

4.1 Mechanical behaviour of baseline fan blade

Static structural, modal and harmonic response analyses are firstly performed for the reference fan blade system to provide the baseline for the fan blade with different viscoelastic patches. The number of modes considered is identified based on the modal participation factor and equivalent mass.

4.1.1 Static structural analysis

The static structural analysis is conducted based on the pressure distribution obtained from the polynomial function. The local maximum principal stress is found to be 668 MPa, as shown in Figure 7, which is an acceptable value as it does not go above the yield strength of Ti-464, which is approximately 1 GPa. Since the local maximum principal stress and the equivalent stresses are found to be acceptable, it is expected that the structural integrity of the design loads is to be preserved.

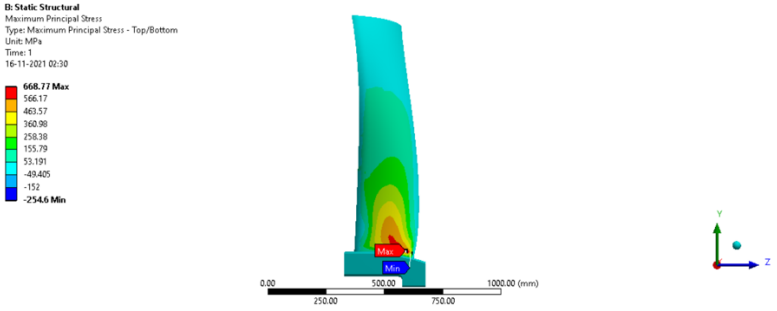

Figure 7: Maximum principal stress distribution

4.1.2 Modal analysis

A preliminary modal analysis of the base structure is performed, and the mode shapes are extracted and plotted in Figure 8. Only the first six modes, which are shown in Table 3, fall within the scope of consideration based on the participation factor summary discussed in the relevant following section. The mode shapes are very much mixed and not to be distinctly identified with the conventional terminology due to the complex geometry.

Table 3: First six natural frequencies and mode shapes of the baseline turbofan blade

Mode	Frequency
1	13.498
2	36.305
3	44.437
4	152.50
5	182.05
6	270.39

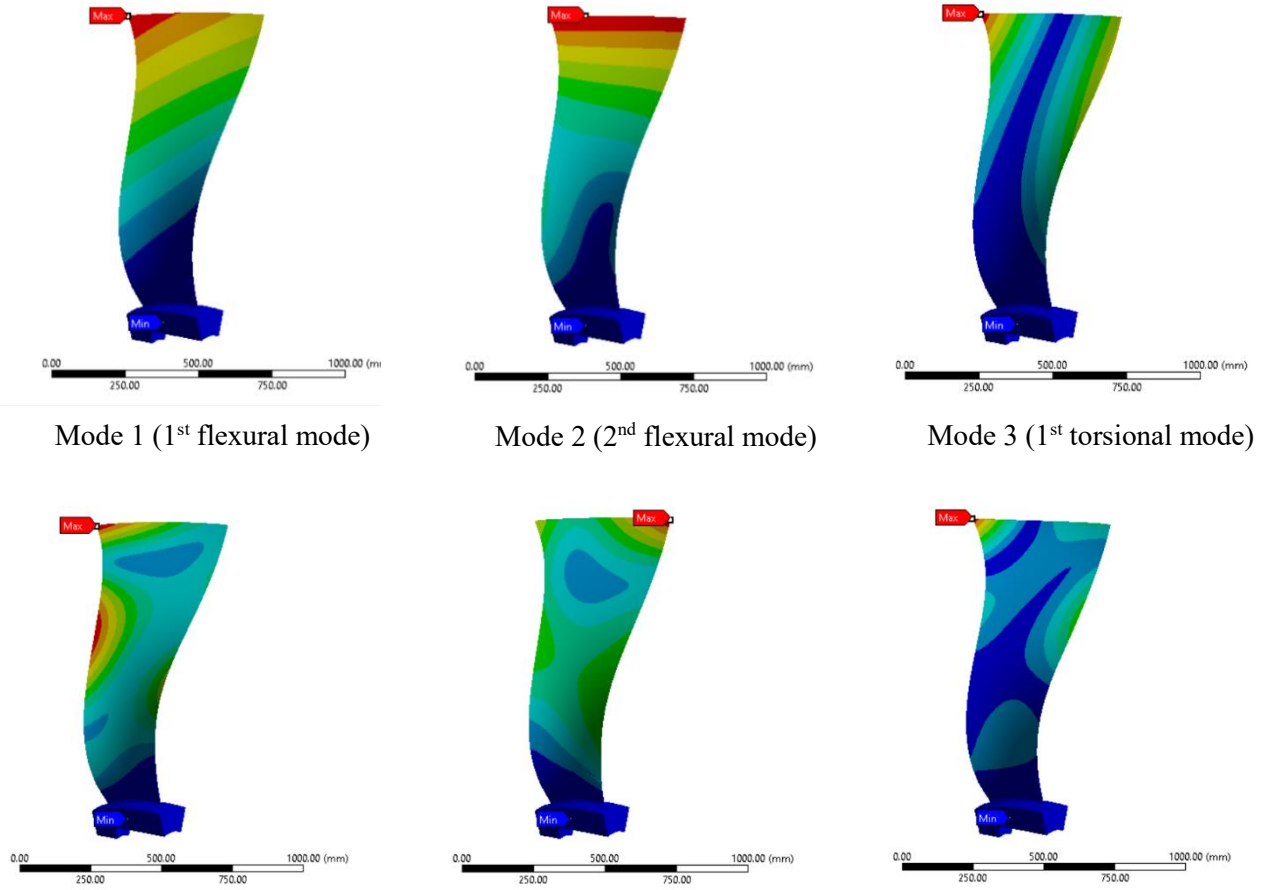

Mode 1 (1st flexural mode) Mode 2 (2nd flexural mode) Mode 3 (1st torsional mode)

Mode 4 (1st Edge-wise mode) Mode 5 (3rd flexural mode) Mode 6 (2nd torsional mode)

Figure 8: The first six mode shapes of the fan blade

4.1.3 Mode participation factor

For the model under consideration, there are, in total 23 904 DOFs. The idea of the modal participation factor is to understand the contribution of each mode to the deformation of the structure under dynamic loads [19]. The modal participation factor and effective mass for the first 15 modes of the baseline fan blades are extracted and shown in Table 4. It is observed that the participation factor and the effective mass for the first six modes contributed significantly to the external disturbances in the system. Also,

it is noted that the first mode defined the highest loads in the fan blade structure, contributing to the largest amplitude response of the system.

Table 4: Modal Participation factor summary in the XYZ cartesian coordinate system

Mode	Frequency(Hz)	X direction	Y direction	Z direction
1	13.498	0.10033	$2.7669\ 10^{-3}$	$-8.1543\ 10^{-3}$
2	36.305	$2.924\ 10^{-2}$	$-6.8056\ 10^{-4}$	$8.1204\ 10^{-2}$
3	44.437	$2.709\ 10^{-2}$	$3.0595\ 10^{-3}$	$-2.4848\ 10^{-2}$
4	152.50	$1.6282\ 10^{-2}$	$-3.4144\ 10^{-2}$	$4.0121\ 10^{-2}$
5	182.05	$-3.8473\ 10^{-2}$	$2.6319\ 10^{-2}$	$3.5189\ 10^{-2}$
6	270.39	$2.2382\ 10^{-2}$	$-4.4559\ 10^{-2}$	$1.9368\ 10^{-2}$
7	315.15	$-5.922\ 10^{-4}$	$1.6955\ 10^{-2}$	$-1.8433\ 10^{-2}$
8	392.88	$-5.9754\ 10^{-3}$	$-2.5361\ 10^{-2}$	$1.8205\ 10^{-2}$
9	484.82	$-8.3654\ 10^{-3}$	$3.1566\ 10^{-2}$	$-2.3972\ 10^{-2}$
10	604.87	$3.0739\ 10^{-3}$	$-4.0539\ 10^{-4}$	$-2.3444\ 10^{-2}$
11	631.45	$-3.0457\ 10^{-3}$	$1.875\ 10^{-2}$	$1.386\ 10^{-2}$
12	704.13	$4.2451\ 10^{-3}$	$-3.1104\ 10^{-2}$	$-2.2097\ 10^{-2}$
13	775.4	$1.2405\ 10^{-3}$	$8.0814\ 10^{-3}$	$8.4046\ 10^{-2}$
14	843.26	$1.6979\ 10^{-3}$	$-4.651\ 10^{-3}$	$-2.23\ 10^{-2}$
15	907.29	$-2.2423\ 10^{-3}$	$-1.5688\ 10^{-2}$	$-1.0705\ 10^{-2}$

4.1.4 Modal strain energy distributions

The modal strain energy distributions for the first six modes under consideration are extracted as depicted in Figure 9. These provide a basis for selecting a suitable region for the application of the viscoelastic patch. Since the modal strain energy technique is an effective method for selecting the locations of the CLD treatment to achieve desired damping performance, the modal strain energy approach is used. For this purpose, the locations are selected where modal strain energy is at its maximum value for a particular mode in order to target and reduce specific modes of vibrations. This is mainly focused on the first mode, where the maximum modal strain energy is close to the root of the fan blade.

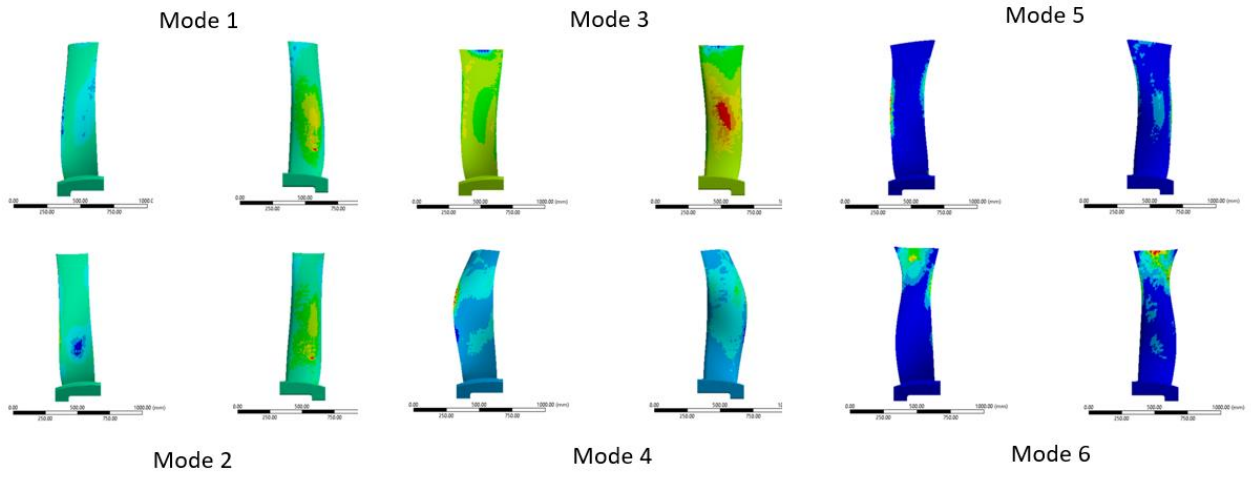

Figure 9: Modal strain energy distribution for the first six modes

4.2 Parametric harmonic response studies of patched turbofan blade

4.2.1 Take-off and landing conditions

The harmonic response analysis is performed for the different damping material candidates and their responses are compared to the baseline are plotted in Figure 10 as an example. The thickness ratio is considered to be 1:1, and a thickness of 0.125 mm for both the constraining and damping layers is considered for the purpose of this analysis. Since the patch thickness is much smaller in comparison with the overall dimensions of the blade, the frequency response shows a minimal reduction of resonance forced response. Figure 11 shows bar graphs of forced frequency amplitude response peaks compared to the baseline for single-layer CLD in take-off conditions showing the vibration damping contribution of individual materials. Both a single bi-layer and a double bi-layer of 0.125 mm thick constraining layer and viscous layer are employed.

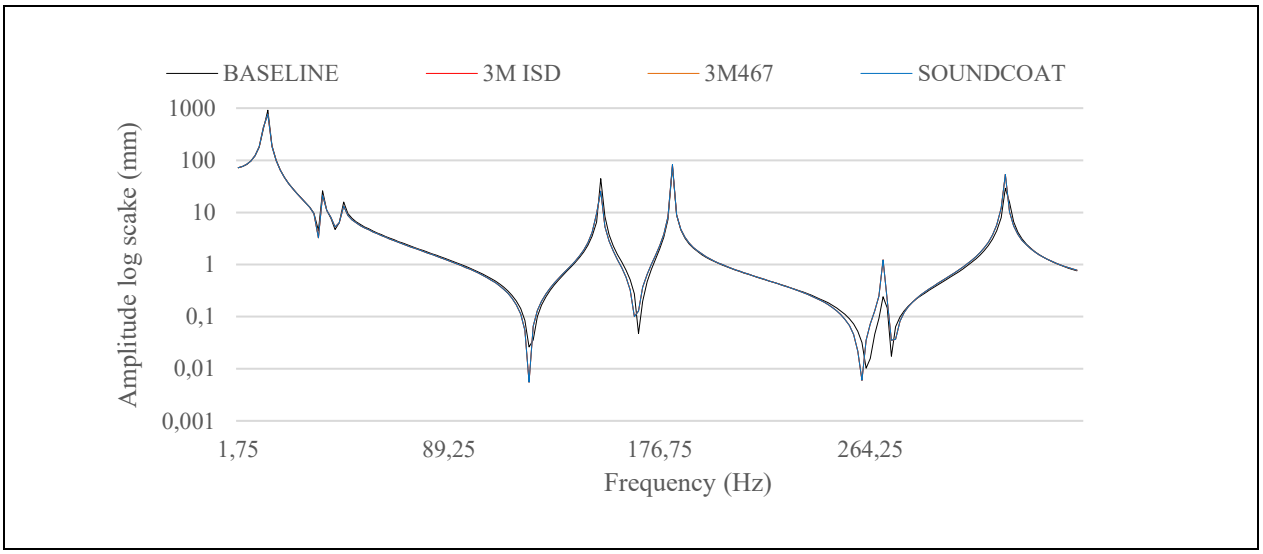

Figure 10: An example of forced frequency amplitude response of fan blade with different viscoelastic patch compared to the baseline

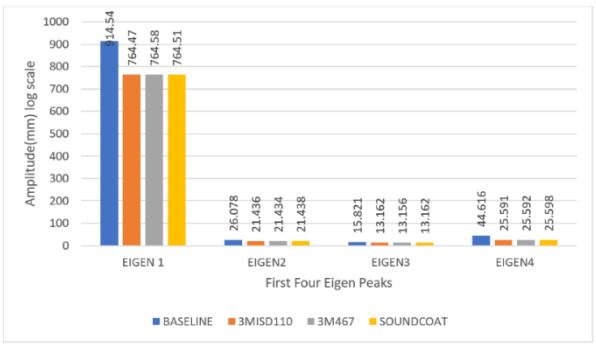

(a)

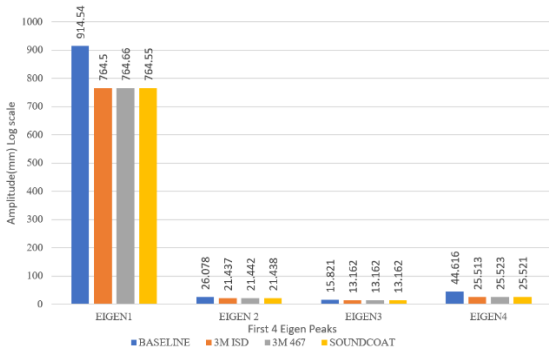

(b)

Figure 11: Harmonic response spectrum for (a) single and (b) double layer patches at take-off and landing

4.2.2 Cruise conditions

The cold case temperature condition is tested in the solver using the damping properties already available from [25]. Same thickness ratios and thickness values are used for the purpose of this set of analyses. The amplitude in the logarithmic scale is plotted on the y-axis against the frequency band for the dynamic analysis of the cruise condition single layer CLD treatment in Figure 12.

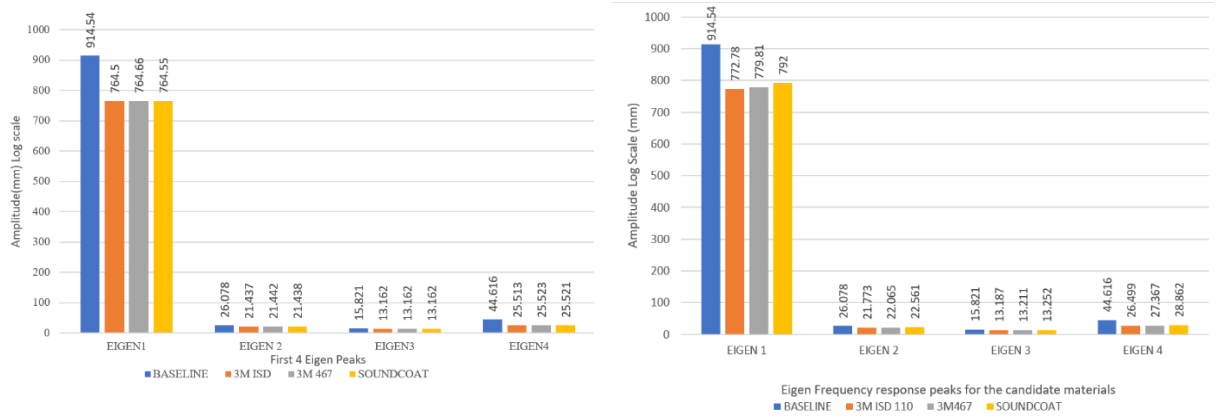

(a) (b)

Figure 12: Harmonic response spectrum for (a)single and (b) double-layer patches in cruise

Figure 13 shows the weighted cost objective of the dynamical response of these three types of constrained damping layers using double layers for both take-off and cruise conditions in the first four modes. From the properties extracted from the forced frequency response, it can be clearly seen that 3MISD110 slightly outperforms other CLD treatment materials.

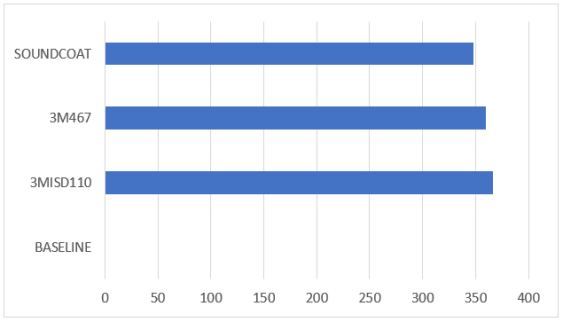

Figure 13: Overall performance of candidate materials using double layer CLD

4.3 Patch location optimisation

It is found from optimisation study that the optimised patch is around 15% of the total surface area of the suction side of the turbofan blade, which is consistent with the modal strain energy plot of the first two modes. The optimised patch location is given in Figure 14.

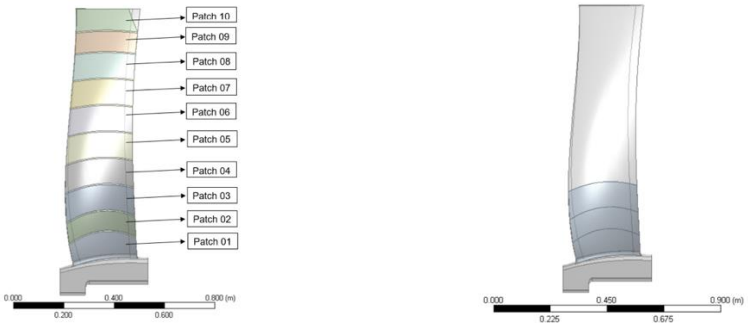

Figure 14: Patch distribution and optimised patch on the fan blade

Figure 15 shows the harmonic response of the fan blade with the optimised turbofan blade patch when a thickness of 0.2 mm is assumed for the patch. It is found that the optimised patch showed significant improvement in damping the resonance peaks with attenuation of the modes at higher natural frequencies (4^{th} and 5^{th}) instead of the modes at a low natural frequency (1^{st}).

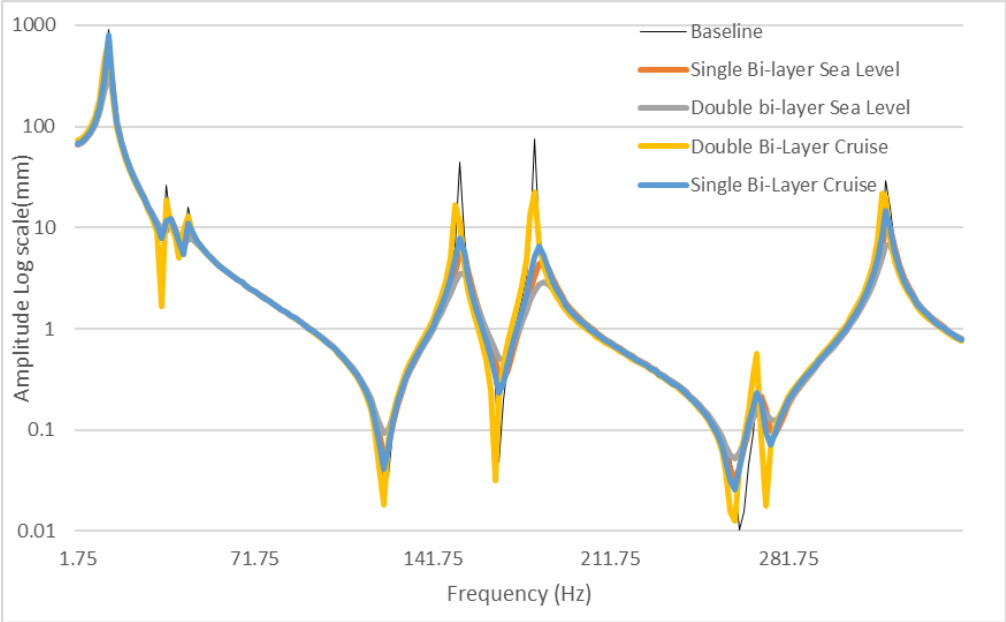

Figure 15: Forced Frequency response comparison of the optimised patch in different conditions including two bilayer configurations

5 Conclusion

The objective of this study is to investigate the feasibility of using viscoelastic materials to mitigate the vibration of a fan blade system. A full-scale 3D turbofan blade finite element model is used for the case study, whose static and dynamic analysis is performed using ANSYS. Three different viscoelastic material-based CLD layers are investigated with two different thicknesses and two different operation temperature conditions. It is found from the modal analysis that the modal properties of applied patch configurations vary slightly from that of the baseline configuration, which is ideal as any significant change of natural frequencies would lead to the risk of resonance because of the high modal density of the fan blade. From the modal participation factor and equivalent mass summaries, it is found that the first six modes contributed significantly to the dynamic response of the system, which is considered in the following dynamical analysis. Out of the three viscoelastic materials under consideration, it is found in harmonical response analysis that 3M-ISD110-based CLD outperformed all the other two candidate materials under

investigation, showing higher performance in both temperature conditions. In terms of the cost function, 3M ISD 110 is found to be 367, whereas all the other materials scored below 350 when compared to the baseline. The topological optimisation study found that an ideal location of the patch is attached to the root, where the strain energy is found to be the maximum for the first two modes. The double bi-layer configuration showed a poor response in cruise condition due to the temperature dependency of the viscoelastic patch that makes it ineffective in viscous shear unloading due to a reduced performance in colder operating temperatures. To be specific, it is found that the optimised patch area is approximately equal to 15 % of the total surface area of the suction side. The optimised patch showed an average 36 % resonance response reduction for the first three modes from the forced frequency response compared to the baseline fan blade.

References

[1] A. F. El-sayed, "Performance Analysis of Cold Sections of High BYPASS Ratio Turbofan Aeroengine," *J. Robot. Mech. Eng. Res.*, vol. 2, no. 1, pp. 18–27, 2017, doi: 10.24218/jrmer.2017.23.

[2] N. Cumpsty, *Jet propulsion*, vol. 14, no. 2. 1942.

[3] A. V Srinivasan, "Flutter and Resonant Vibration Characteristics of Engine Blades: An IGTI Scholar Paper," *ASME 1997 International Gas Turbine and Aeroengine Congress and Exhibition*. Jun. 02, 1997, doi: 10.1115/97-GT-533.

[4] J. S. RAO, "Tubomachine blade vibration," *Shock Vib. Dig.*, vol. 19, no. 5, pp. 3–10, 1987.

[5] B. A. Cowles, "High cycle fatigue in aircraft gas turbines—an industry perspective," *Int. J. Fract.*, vol. 80, no. 2, pp. 147–163, 1989, doi: 10.1007/BF00012667.

[6] Z. Liu, Z. Chen, and J. Chen, "The Strength Analysis of CFM56 Engine Blade," *MATEC Web Conf.*, vol. 166, pp. 2–5, 2018, doi: 10.1051/matecconf/201816604001.

[7] L. Salles, and M. Vahdati. "Comparison of two numerical algorithms for computing the effects of mistuning of fan flutter." *Turbo Expo: Power for Land, Sea, and Air*. Vol. 49842. American Society of Mechanical Engineers, 2016.

[8] L. Salles, L. Blanc, F. Thouverez, A. M. Gouskov, and P. Jean, "Dynamic Analysis of a Bladed Disk With Friction and Fretting-Wear in Blade Attachments," *ASME Turbo Expo 2009: Power for Land, Sea, and Air*. pp. 465–476, Jun. 08, 2009, doi: 10.1115/GT2009-60151.

[9] T. M. Young, "International Standard Atmosphere (ISA) Table," *Perform. Jet Transp. Airpl. Anal. Methods, Flight Oper. Regul.*, pp. 583–590, Nov. 2017, doi: 10.1002/9781118534786.APP1.

[10] J. Yuan, G. Allegri, and F. Scarpa, " Buffeting mitigation using carbon nanotube composites: a feasibility study", *Proceedings of the Institution of Mechanical Engineers, Part G: Journal of Aerospace Engineering*, 227(9), pp.1425-1440, 2013

[11] R. Muki and E. Sternberg, "On Transient Thermal Stresses in Viscoelastic Materials With Temperature-Dependent Properties," *J. Appl. Mech.*, vol. 28, no. 2, pp. 193–207, Jun. 1961, doi: 10.1115/1.3641651.

[12] M. Gröhlich, A. Lang, M. Böswald, and J. Meier, “Viscoelastic damping design – Thermal impact on a constrained layer damping treatment,” *Mater. Des.*, vol. 207, 2021, doi: 10.1016/j.matdes.2021.109885.

[13] Y. Gao, Y. Zhou, and X. Sun, "Engine vibration certification," *Procedia Eng.*, vol. 80, pp. 1–9, 2014, doi: 10.1016/j.proeng.2014.09.053.

[14] Y. Sun, J. Yuan, E. Denimal, and L. Salles, "Nonlinear Modal Analysis of Frictional Ring Damper for Compressor Blisk," *ASME Turbo Expo 2020: Turbomachinery Technical Conference and Exposition*. Sep. 21, 2020, doi: 10.1115/GT2020-14277.

[15] A. Lupini and B. I. Epureanu, "A friction-enhanced tuned ring damper for bladed disks," *J. Eng. Gas Turbines Power*, vol. 143, no. 1, 2021, doi: 10.1115/1.4049203.

[16] M. H. Jareland, "The Use of Platform Dampers to Reduce Turbine Blade Vibrations," no. 872, pp. 1–28, 2001, [Online]. Available: https://www.osti.gov/etdeweb/servlets/purl/20152200#:~:text=Friction damping is commonly used,the reliability of the engine.&text=A platform damper is a,underneath two adjacent blade platforms.

[17] D. Collins, "Vibration damping: What's the difference between passive and active?" https://www.motioncontroltips.com/vibration-damping-whats-the-difference-between-passive-and-active-methods/ (accessed Nov. 10, 2021).

[18] L. Hazard, "Design of viscoelastic damping for vibration and noise control : modelling , experiments and optimisation Design of viscoelastic damping for vibration and noise control : modelling ," 2007.

[19] A. C. Galucio, J. F. Deü, and R. Ohayon, "A fractional derivative viscoelastic model for hybrid active-passive damping treatments in time domain - Application to sandwich beams," *J. Intell. Mater. Syst. Struct.*, vol. 16, no. 1, pp. 33–45, 2005, doi: 10.1177/1045389X05046685.

[20] M. A. Trindade and A. Benjeddou, "Hybrid active-passive damping treatments using viscoelastic and piezoelectric materials: Review and assessment," *JVC/Journal Vib. Control*, vol. 8, no. 6, pp. 699–745, 2002, doi: 10.1177/1077546029186.

[21] X. D. Zhang and C. T. Sun, "Formulation of an adaptive sandwich beam," *Smart Mater. Struct.*, vol. 5, no. 6, pp. 822–823, 1996, doi: 10.1088/0964-1726/5/6/012.

[22] D. Rodrigues, "Vibroacoustic Analysis of Plates with Damping Patches Using a Layerwise Theory and the Rayleigh-Ritz Method," pp. 15–17, 2014.

[23] J. F. Shepherd and C. R. Johnson, "Hexahedral mesh generation constraints," *Eng. Comput.*, vol. 24, no. 3, pp. 195–213, 2008, doi: 10.1007/s00366-008-0091-4.

[24] A. Loredo, A. Plessy, A. El Hafidi, and N. Hamzaoui, "Numerical vibroacoustic analysis of plates with constrained-layer damping patches," *J. Acoust. Soc. Am.*, vol. 129, no. 4, p. 1905, Apr. 2011, doi: 10.1121/1.3546096.

[25] D. Hozić, "Mechanical loads on a turbofan engine structure at blade-off," p. 92, 2009.

[26] M. Tufekci, Q. Rendu, J. Yuan, J. P. Dear, L. Salles, and A. V. Cherednichenko, "Stress and modal analysis of a rotating blade and the effects of nonlocality," *Proc. ASME Turbo Expo*, vol. 10B-2020, no. September, 2020, doi: 10.1115/GT2020-14821.